Free Radical Biology and Medicine 152 (2020) 348–354

Contents lists available at ScienceDirect

Free Radical Biology and Medicine

journal homepage: www.elsevier.com/locate/freeradbiomed

Original article

DNA glycosylase Neil2 contributes to genomic responses in the spleen during clinical prion disease

Katja Scheffler[a,b,c,d,*], Clara M.O. Jalland[e], Sylvie L. Benestad[f], Torfinn Moldal[f], Cecilie Ersdal[g], Gjermund Gunnes[e], Rajikala Suganthan[h], Magnar Bjørås[b,d,h], Michael A. Tranulis[e]

[a] Department of Neuromedicine and Movement Science, Norwegian University of Science and Technology, Trondheim, Norway
[b] Department of Clinical and Molecular Medicine, Norwegian University of Science and Technology, Trondheim, Norway
[c] Department of Neurology, St. Olavs Hospital, Trondheim, Norway
[d] Department of Laboratory Medicine, St. Olavs Hospital, Trondheim, Norway
[e] Department of Basic Sciences and Aquatic Medicine, Faculty of Veterinary Medicine, Norwegian University of Life Sciences, Campus Adamstuen, Oslo, Norway
[f] Norwegian Veterinary Institute, Oslo, Norway
[g] Department of Production Animal Clinical Sciences, Faculty of Veterinary Medicine, Norwegian University of Life Sciences, Campus Sandnes, Norway
[h] Department of Microbiology, Oslo University Hospital and University of Oslo, Norway

A B S T R A C T

The DNA glycosylase Neil2 is a member of the base excision repair (BER) family of enzymes, which are important for repair of oxidative DNA damage. Specifically, Neil2 participates in repair of oxidized bases in single-stranded DNA of transcriptionally active genes. Mice with genetic ablation of Neil2 (*Neil2*$^{-/-}$) display no overt phenotypes, but an age-dependent accumulation of oxidative DNA damage and increased inflammatory responsiveness. In young mice intra-cerebrally inoculated with prions, vigorous prion propagation starts rapidly in the germinal follicles of the spleen due to inoculum spillover. Here, we compare experimental prion disease in *Neil2*$^{-/-}$ mice with that in wild-type mice at disease onset and end-stage. Specifically, we investigated disease progression, accumulation of DNA damage, and mitochondrial respiratory complex activity in brain and spleen. We used genome-wide RNA sequencing of the spleen to compare the immune responses to prion propagation between the two groups of mice, at both onset and end-stage prion disease. The *Neil2*$^{-/-}$ mice deteriorated more rapidly than wild-type mice after onset of clinical signs. Levels of DNA damage in brain increased in both mouse groups, slightly more in the *Neil2*$^{-/-}$ mice. Transcriptome data from spleen at disease onset were similar between the mouse groups with moderate genomic responses. However, at end-stage a substantial response was evident in the wild-type mice but not in *Neil2*$^{-/-}$ mice. Our data show that Neil2 counteracts toxic signaling in clinical prion disease, and this is separate from gross pathological manifestations and PrP^{Sc} accumulation.

1. Introduction

Prion diseases are invariably fatal, neurodegenerative maladies caused by disease-provoking protein complexes, known as prions. These consist of misfolded conformers of the host-encoded cellular prion protein PrP^{C} [1,2]. The pathogenic aggregates often display some protease resistance and are known as PrP^{Sc} when revealed in immunohistochemistry or western blots. In some naturally occurring prion diseases, such as classical scrapie in sheep and chronic wasting disease in deer, PrP^{Sc} aggregates are often abundantly present in peripheral lymphoid tissues along the gastrointestinal tract and in the spleen long before onset of clinical signs [3–5].

In experimental prion disease in mice, induced by intracerebral inoculation with the mouse-adapted scrapie strain RML (Rocky Mountain Laboratory), a similar situation occurs, with vivid peripheral prion propagation in the spleen that is probably initiated by inoculum spillover [6]. It has long been known that prions propagate in the spleen [7,8] and that peak infectivity levels are reached much faster in spleen than in brain [9,10]. The facility of prion propagation in the spleen is also of importance regarding cross species [11] transmission as well as strain developments [12,13]. The tissue fixed follicular dendritic cells, which are located in the white pulp germinal centers is of pivotal importance for prion propagation in the spleen [14,15] and PrP^{Sc} accumulations are mainly located in these follicles. In accordance with this, we have also observed active prion propagation in the spleen in RML-infected mice that are compromised regarding repair of oxidative DNA damage. Animals express a battery of DNA repair glycosylases with overlapping activities, especially in the base excision repair (BER) pathway [16,17]. Interestingly, genetic disruption of BER enzymes generally reveals no overt phenotypes related to genomic instability or cancer development. The full range of physiological roles of BER enzymes is incompletely understood and probably goes beyond canonical DNA repair and maintenance of genomic quality [18]. However, gene knockout of downstream effectors, such as APE1 or pol β are embryonic

* Corresponding author. Department of Neuromedicine and Movement Science, Norwegian University of Science and Technology, Trondheim, Norway.
E-mail address: katja.scheffler@ntnu.no (K. Scheffler).

https://doi.org/10.1016/j.freeradbiomed.2020.03.030
Received 21 February 2020; Received in revised form 19 March 2020; Accepted 29 March 2020
Available online 04 April 2020

lethal, suggesting that accumulation of BER pathway intermediates is lethal [19–21].

RML prion disease in mice with combined knock-out of the DNA repair enzymes 8-oxoguanine and mutY DNA glycosylase, *Ogg1*$^{-/-}$ and *Mutyh*$^{-/-}$, and in mice with disruption of the Nei endonuclease VIII-like 3 gene, *Neil3*$^{-/-}$, indicates that DNA glycosylases contribute to neuroprotection during the clinical stages of neurodegeneration without altering overall disease features [22,23]. Here we have used the same experimental paradigm to address prion disease development in mice that lack expression of the DNA glycosylase Neil2 (*Neil2*$^{-/-}$). Since these mice have been shown to be hyper-responsive to certain forms of inflammatory insults [24], we were particularly interested in studying prion disease progression in the spleen, in addition to brain pathology.

2. Materials and methods

Ethics statement: All animal work was carried out in accordance with the European Convention for the Protection of Vertebrate Animals Used for Experimental and Other Scientific Purposes and according to Norwegian Regulations of Animal Experimentation (FOTS). Approval number 6232.

Mice: In these experiments, 34 female mice, 20C57Bl/6Y (wild-type) and 14 transgenic *Neil2*$^{-/-}$ mice, were inoculated intra-cerebrally with the RML isolate. All mice were female and weighed between 18 and 22 g at inoculation. Two wild-type mice that died two days after inoculation were excluded from the experiment. One wild-type mouse was found dead 156dpi, but material was of insufficient quality for further diagnosis and analysis. Four wild-type mice and three *Neil2*$^{-/-}$ mice served as non-inoculated age-matched controls for the DNA-damage analysis. Wild-type C57Bl/6 mice were bred in-house in the same room as *Neil2*$^{-/-}$ mice. Mice were maintained in high grade facility under a 12-h light/12-h dark cycle at 21 °C, with food and water ad libitum, and housed in groups of four in individually ventilated and sealed cages. Breeding of the animals was done in accordance with European regulations FELASA category C. The genotypes of the mice were assessed by a PCR-based protocol.

Inoculum: Mice were inoculated with the mouse adapted scrapie strain RML, which is originally derived from sheep scrapie brain homogenate (SSBP-1). RML has been passaged in many lines of mice and adapted into C57Bl/6Y. Anesthesia was achieved with a mixture of tiletamine, zolezepam and xylazine, which was injected subcutaneously. Mice were intracerebrally inoculated, into the right mid-hemisphere, with a 20 µl of a 10% inoculum.

Monitoring and sampling: The animals were monitored daily. Signs of clinical disease, such as stiff tail, ataxia, ruffled coat, hyperexcitability, kyphosis, hind leg paresis, trembling, and lethargy, were recorded.

In order to characterize the progression of disease, animals were sacrificed at onset and end-stage of disease. In total, 15 animals, 9 wild-type and 6 transgenic *Neil2*$^{-/-}$ mice were euthanized at onset of early clinical signs. At the predefined clinical endpoint, 10 wild-type and 6 transgenic *Neil2*$^{-/-}$ mice were sacrificed and the material was collected. The brain was cut in two halves. One half was fixed in 10% neutral buffered formalin, and later used for immunohistochemistry (IHC). The other half was either frozen and later used for detection of PrP^{Sc} by Western blot (WB), DNA damage analysis and RNA sequencing or immediately processed for mitochondrial isolation.

Lesion scoring and immunohistochemistry: After fixation, the brain tissue was cut into five transverse sections [25] and embedded in paraffin. Sections (4 µm thickness) were routinely stained with haematoxylin and eosin (HE) and blindly scored for lesion profiling by two pathologists as described previously [22,23].

For histological detection of PrP^{Sc}, the sections were pretreated by immersion in 98% formic acid for 30 min, washed and autoclaved at 121 °C in 0.01 M citric acid, pH 6.1 for 30 min, prior to incubation with proteinase K (4 µg/mL) at 37 °C for 5 min. The primary antibodies (F89/160.1.5 1/2000 and 2G11 1:400) was applied for 1 h at room temperature. To detect PrP^{Sc}, a commercially available kit (EnVision® + System–HRP (AEC) Mouse, DAKO) was used.

Pet Blot: Brain and spleen tissue was cut (3–5 µm) from paraffin imbedded tissue and placed on 0.45 µm nitrocellulose membrane, with glass slide underneath, and dried for approximately 1 day. The membranes were deparaffinized, rehydrated and placed in buffer with 250 µg/mL Proteinase K (Sigma-Aldrich) on top of towel paper, pillow technique, overnight at 55 °C. The membranes were washed with Tris-buffered saline with 0.1% Tween 20, before denaturation in 4 M guanidiumthiocynate for 15 min and washed 3 × 5 min with TBST. Membranes were blocked in 0.2% casein in PBS with 0.1% Tween 20 for 45 min, and incubated with primary antibody, Sha31, for 90 min at room temperature. Secondary antibody, goat anti-mouse labeled with alkaline phosphatase, in TBST was applied for 60 min. The signals were visualized through Formazan reaction with NBT/BCIP. The staining process was stopped by incubation of the sections in PBS for 15–30 min. To achieve a long-lasting staining the membranes were incubated in ddH_2O and 0.5 M EDTA for 1–2 h.

Western blot analysis for detection of PrP^{Sc}: To detect PrP^{Sc}, the brain samples were homogenized at room temperature in a buffer containing Tris-HCl pH 7.4, 150 mM NaCl, 0.5% (w/v) Triton X-100, 0.5% sodium deoxycholate, and treated with Proteinase K (4 µg/mL) for 1 h at 37 °C, or with PNGase F (New England Biolabs) for 2 h at 37 °C for deglycosylation. PK digestion was stopped by adding SDS sample buffer and boiling the samples at 95 °C for 5 min. Proteins were separated on 12% pre-cast polyacrylamide gels (Bio-Rad) and transferred to polyvinylidene fluoride membranes by a semi-dry blotter. Membranes were blocked in 5% fat-free dry milk for 1 h, before incubation with primary antibody, Bar224 (Spi Bio, France), overnight at 4 °C. Secondary antibody (goat anti-mouse) labeled with alkaline phosphatase (ALP: GE Healthcare, UK) was applied to visualize bands with a fluorescence imager (Typhoon 9200, GE Healthcare, UK) after incubation with the ALP substrate (ECFTM, Western blotting reagent pack, GE Healthcare). According to the recommendations of the manufacturers, an EU and OIE approved test, (TeSeE WESTERN BLOT, Bio-Rad) was used. The immunodetection was performed using the monoclonal antibody SHa31 that recognizes the amino acids (YEDRYYRE), corresponding to codons 145–152 in human PrP. Peroxidase activity was revealed using enhanced chemiluminescence (ECL, GE Healthcare, UK) substrate.

Mitochondrial complex activity analyses: Mitochondria from freshly prepared tissue samples were isolated and complex I and V activity measured as described previously [26].

Nucleic acid extraction: Tissue samples were stored in RNAlater Stabilization solution (Invitrogen) for at least 24 h before homogenization with FastPrep-24 (MP Biomedical). Genomic DNA and total RNA were isolated using the Allprep DNA/RNA/Protein isolation kit (Qiagen).

RT-qPCR: cDNA was synthesized from 1 µg total RNA using the High Capacity cDNA Reverse Transcription Kit (Applied Biosystems). Gene expression of DNA glycosylases were measured using the following primers: *Neil1*, forward: 5′ GCTGACCCTGAGCCAGAAGAT 3′ and reverse: 5′ CCCCAACTGGACCACTTCCT 3′, *Neil2*, forward: 5′ TTT AGTGGTGGTGGCTTCCT 3′ and reverse: 5′ TGATGTTCCCTAATCCTG AGAAG 3′, *Neil3* forward: 5′ GGGCAACATCATCAAAAATGAA 3′ and reverse: 5′ CTGTTTGTCTGATAGTTGACACACCTT 3′, *Nth1*, forward: 5′ CCCGGAGCCGTTGCA 3′ and reverse: 5′ TGCTCTCCAGCCAGACCAA 3′, *Ogg1*, forward: 5′GTGACTACGGCTGGCATCC 3′ and reverse: 5′ AGGC TTGGTTGGCGAAGG 3’. Relative expression levels were calculated using the comparative Δct method and related to the housekeeping gene *ß-actin*.

RNA sequencing: Total RNA from spleen of wild-type (n = 4–6) and *Neil2*$^{-/-}$ mice (n = 4) from control, onset, and end-stage were pooled and sent to BGI Tech Solutions, Hong Kong, for RNA sequencing and bioinformatics analysis. Differentially expressed genes (DEGs) were

filtered using log2Ratio ≥ 1 and false discovery rate (FDR) ≤ 0.001 as cut off. Comparison of DEGs was performed by using Venny 1.0 online tool (http://bioinfogp.cnb.csic.es/tools/venny/index.html). Ingenuity pathway analysis (IPA) software was used to identify enriched pathways and upstream regulator of DEGs.

Nuclear and mitochondrial DNA damage detection: Real-time qPCR was used to quantify nuclear and mitochondrial DNA damage as described in Ref. [27]. Briefly, genomic DNA was digested with Taq$^{\alpha}$I restriction enzyme and subsequent real-time PCR was carried out to amplify non-damaged DNA with site-specific nuclear and mitochondrial DNA primer. Relative amounts of PCR products were calculated by the comparative ΔC_T method. The following primers were used: *Gapdh*, forward: 5′- CTTCAACAGCAACTCCCACT and reverse 5′-AAAAGTCAG GTTTCCCATCC, mt-*Rnr1*, forward: 5′-ACTCAAAGGACTTGGCGGTA and reverse, 5′-AGCCCATTTCTTCCCATTTC.

LC-MS/MS quantification of DNA base modification: DNA samples were digested by incubation with a mixture of nuclease P1 from Penicillium citrinum (Sigma, N8630), DNaseI (Roche, 04716728001) and ALP from *E. coli* (Sigma P5931) in 10 mM ammonium acetate buffer pH 5.3, 5 mM MgCl2 and 1 mM CaCl2 for 30 min at 40 °C. The samples were methanol precipitated, supernatants were vacuum centrifuged at room temperature until dry and dissolved in 50 µl of water for LC/MS/MS analysis. Quantification was performed with an LC-20AD HPLC system (Shimadzu) coupled to an API 5000 triple quadrupole (ABSciex) operating in positive electrospray ionization mode. The chromatographic separation was performed with the use of an Ascentis Express C18 2.7 µm 150 × 2.1 mm i.d. column protected with an Ascentis Express Cartridge Guard Column (Supelco Analytical) with an Exp Titanium Hybrid Ferrule (Optimize Technologies Inc.). The mobile phase consisted of A (water, 0.1% formic acid) and B (methanol, 0.1% formic acid) solutions. The following conditions were employed for chromatography: for unmodified nucleosides – 0.13 mL/min flow, starting at 10% B for 0.1 min, ramping to 60% B over 2.4 min and re-equilibrating with 10% B for 4.5 min; for 5-me(dC) - 0.14 mL/min flow, starting at 5% B for 0.1 min, ramping to 70% B over 2.7 min and re-equilibrating with 5% B for 5.2 min; for 5-hm(dC), 5oh(dC), and 8-oxo (dG) - 0.14 mL/min flow, starting at 5% B for 0.5 min, ramping to 45% B over 8 min and re-equilibrating with 5% B for 5.5 min. For mass spectrometry detection the multiple reaction monitoring (MRM) was implemented using the following mass transitions: 252.2/136.1 (dA), 228.2/112.1 (dC), 268.2/152.1 (dG), 243.2/127.0 (dT), 242.1/126.0 [5-me(dC)], 258.1/142.0 [5-hm(dC)], 244.1/128 [5-oh(dC)], 284.1/168.1 [8-oxo(dG)].

Statistical analysis: Graphical presentations and statistical analyses were performed with the GraphPad Prism 8 software package. *P*-values < 0.05 were considered statistically significant. Kaplan-Meier survival plots were compared with Log Rank Mantel Cox test, whereas mean values of DNA damage, mitochondrial function, morphometric data and gene expression comparisons were analyzed by two-way ANOVA using Sidak post-hoc analysis to correct for multiple comparison. The *P*-values, in RNA sequencing, were calculated using Fisher's exact test.

3. Results

3.1. Prion disease progression

Pre-inoculation steady state levels of brain PrP^{C} glycoforms and major processing fragment C1 were similar between the mouse genotypes (Fig. 1A). At onset and end-stage prion disease both mouse groups accumulated similar levels of PrP^{Sc}, and the glycoforms were indistinguishable (Fig. 1B). In line with our previous findings of BER pathway compromised mice [22,23], analysis of brain lesion profiles revealed no difference between the genotypes (data not shown).

Although the first clinical signs appeared simultaneously in the two genotype mouse groups, the *Neil2*$^{-/-}$ mice had faster disease progression and were sacrificed according to human end-point relatively synchronously. In the wild-type mice, however, disease progressed more slowly, and some animals had still not been sacrificed more than 20 days after onset of clinical signs (Fig. 1C). In accordance with a more protracted clinical disease, the wild-type mice suffered greater reduction in body mass from onset to end-stage of disease, with a 24% mean reduction in body mass, whereas the *Neil2*$^{-/-}$ dropped 11% of their body mass from onset to end-stage (Fig. 1 D).

3.2. DNA damage analysis

Analysis of genome-wide accumulation of oxidized base lesions in brain showed no difference between *Neil2*$^{-/-}$ and wild-type mice (Fig. S1A). In spleen, levels of 8oxodG and 5ohdC were slightly reduced at onset compared to control but significantly only in Neil2 deficient mice (Fig. S1B). We found no difference in nuclear DNA (nDNA) and mitochondrial DNA (mtDNA) damage level in brain between the mouse genotypes, although mtDNA damage accumulated significantly during disease development (Fig. 2A). In contrast, *Neil2*$^{-/-}$ showed significantly less mtDNA damage in spleen at end-stage than was found in wild-type whereas nDNA damage were indistinguishable between the genotypes (Fig. 2B). As shown in Table 1, the loss of Neil2 activity did not result in upregulation of other DNA glycosylases in the spleen. At onset and end-stage prion disease there was a significant reduction in expression levels of Neil3 DNA glycosylases in both genotype groups.

3.3. Mitochondrial function

Enzymatic activity of complex I in isolated mitochondria from brain was stable during the course of disease, whereas complex V activity slightly increased only in wild-type brain at end-stage compared with onset (Fig. 3A). Interestingly, mitochondrial respiratory activity in *Neil2*$^{-/-}$ spleen was significantly increased at end-stage, both for complex I and complex V, whereas in wild-type mice this upregulation was absent (Fig. 3B).

3.4. RNA sequencing analysis

Transcriptome changes were evident at onset of the disease, with 373 and 384 DEGs in wild-type and *Neil2*$^{-/-}$ spleens respectively, as compared with un-inoculated controls. At end-stage, wild-type mice dramatically increased in DEGs, with 582 upregulated and 1379 downregulated genes, in contrast to *Neil2*$^{-/-}$ mice that had minor differences in number of DEGs at end-stage compared with onset (Fig. 4A). In addition, *Neil2*$^{-/-}$ DEGs overlapped almost 60% with wild-type DEGs at end-stage, suggesting a lack of transcriptional response in *Neil2*$^{-/-}$ spleen at end-stage of prion disease (Fig. 4A and B). The top five significantly affected pathways included cell cycle, proliferation, and DNA replication and repair processes (Fig. 4C). Interestingly, DEGs from *Neil2*$^{-/-}$ spleen at end-stage were enriched in proliferation of immune cells, such as leukocytes and lymphocytes (Fig. 4D). In addition, upstream regulators involved in cell cycle control and DNA damage response were commonly downregulated whereas proliferation processes were activated at end-stage, indicating enhanced proliferation of immune cells in *Neil2*$^{-/-}$ spleen. However, wild-type mice showed, in contrast, inhibition of proliferation and activation of cell cycle control in response to DNA damage during the course of disease (Fig. 4E). Moreover, the transcriptome data demonstrated that genes involved in mitochondrial function were significantly upregulated in *Neil2*$^{-/-}$ spleen at end-stage. We found DEGs contributing both to complex I and complex V activity and several regulators of mitochondrial transcription and translation, including transcription factor B1, mitochondrial translational initiation factor 2 and several mitochondrial ribosomal proteins. These genes, in contrast, were downregulated in wild-type spleen, comparing un-inoculated controls with end-stage mice (Fig. 4F).

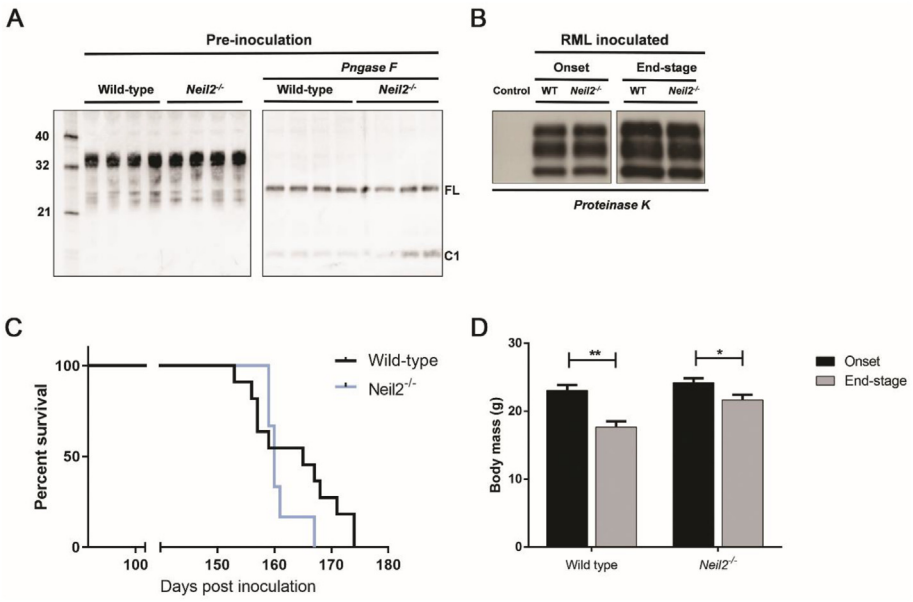

Fig. 1. Pre-inoculation levels of PrP^C, glycoforms, C1 fragment and major disease characteristics in wild-type and *Neil2*$^{-/-}$ mice. A) Steady-state levels of brain PrP^C levels, glycoforms and proteolytic processing were similar between the genotypes. B) Western Blot of brain PrP^{Sc} at onset and end-stage. C) Survival plot of wild-type (n = 11) and *Neil2*$^{-/-}$ (n = 6) mice after inoculation with RML prions. D) Body mass of wild-type and *Neil2*$^{-/-}$ (means ± SEM, n = 6–11 per group) mice at onset and end-stage of prion disease. ** (P < 0.01), * (P < 0.05), Student's t-test.

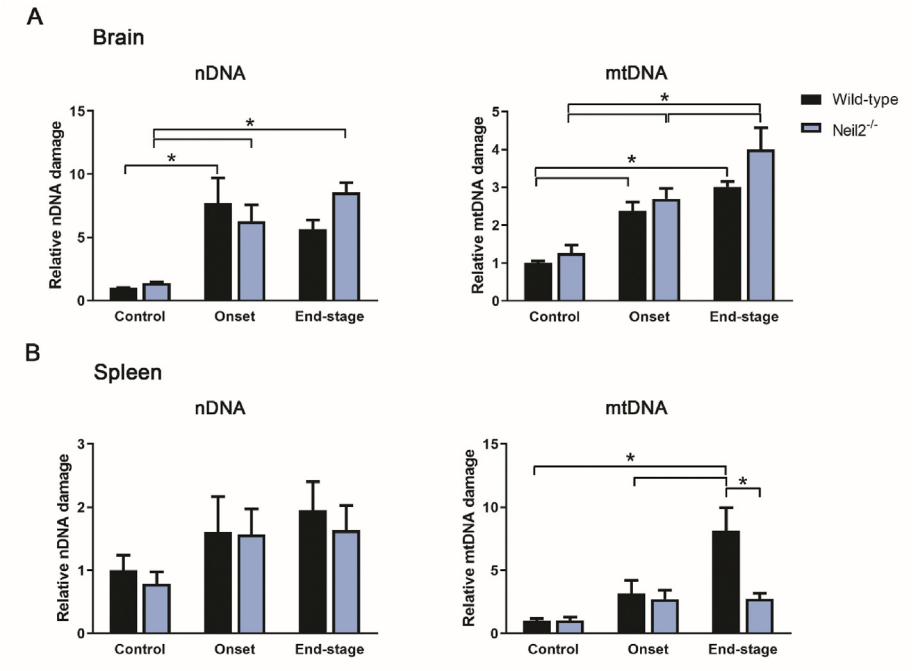

Fig. 2. Mitochondrial DNA damage is decreased in spleen of *Neil2*$^{-/-}$ mice at end-stage of prion disease. Quantitative PCR-based analysis of nuclear DNA (nDNA) and mitochondrial DNA (mtDNA) damage in A) brain and B) spleen in controls and RML-inoculated wild-type and *Neil2*$^{-/-}$ mice. Data presented as means (n = 3–6 per group and time-point), +/− SEM. * (P < 0.05).

4. DNA methylation analysis

Global genomic levels of 5 mC dropped significantly at onset of disease in wild-type and *Neil2*$^{-/-}$ spleen. However, wild-type mice maintained similar levels of 5 mC at end-stage compared with onset, whereas at end-stage in *Neil2*$^{-/-}$ mice 5 mC levels returned to the level of un-inoculated controls (Fig. 5A). In comparison, 5hmC slightly increased during disease progression in wild-type spleen, but not in

Table 1
Relative gene expression of DNA glycosylases in spleen.

Gene	Wild-type			Neil2$^{-/-}$		
	Control	Onset	End-stage	Control	Onset	End-stage
Neil1	1,00 ± 0.20	1,24 ± 0.12	0,69 ± 0.15[b]	1109 ± 0.13	0,960 ± 0.04	0,778 ± 0.09
Neil2	1,00 ± 0.17	0,76 ± 0.09	1,46 ± 0.32	–	–	–
Neil3	1,00 ± 0.25	0,31 ± 0.04[a]	0,18 ± 0.04[a]	0,764 ± 0.15	0,277 ± 0.05[a]	0,232 ± 0.07[a]
Nth1	1,00 ± 0.18	0,88 ± 0.07	1,00 ± 0.09	0,891 ± 0.10	0,743 ± 0.05	0,823 ± 0.04
Ogg1	1,00 ± 0.08	1,00 ± 0.07	0,93 ± 0.02	0,931 ± 0.09	0,810 ± 0.05	0,828 ± 0.05

p < 0.05 vs control[a] or vs onset.[b].

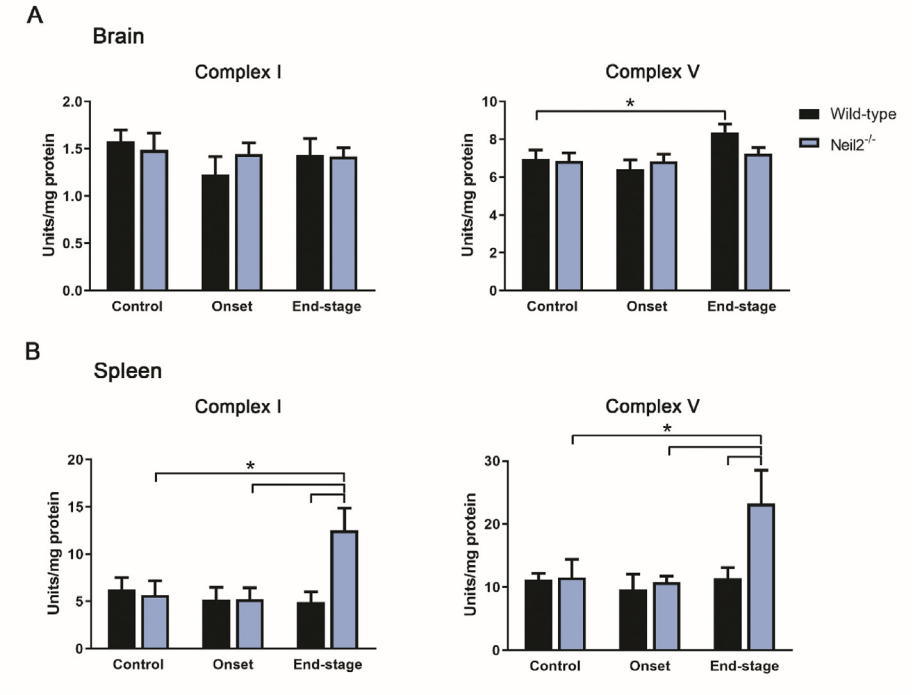

Fig. 3. Mitochondrial burst in spleen of *Neil2*$^{-/-}$ mice at end-stage of prion disease. Mitochondrial function was analyzed in brain and spleen of un-inoculated and RML-inoculated wild-type and *Neil2*$^{-/-}$ mice at onset and end-stage of disease. A) Assessment of brain and B) spleen mitochondrial complex I and complex V activity in controls and RML-inoculated wild-type and *Neil2*$^{-/-}$ mice. Data presented as means (n = 3–6 per group and time-point), +/− SEM. * (P < 0.05).

Neil2$^{-/-}$ spleen (Fig. 5B). The effects on epigenetic modifications were specific for spleen; brain levels of 5 mC and 5hmC were stable during the disease and similar between the genotypes (Fig. S2).

4.1. Spleen histopathology

There were no gross pathological differences in the spleen between *Neil2*$^{-/-}$ mice and wild-type and the overall splenic architecture appeared intact (Fig. 6). At end-stage, amyloid masses were evident in the center of splenic follicles and this appeared slightly more pronounced in the *Neil2*$^{-/-}$ mice (Fig. 6 panels B and E), but limitations in material prevented quantification. Paraffin embedded tissue blots (PET) demonstrated prominent follicular PrP^{Sc} deposits that appeared similar between the genotypes (Fig. 6 panels C and F).

5. Discussion

As has previously been observed in experimental prion disease in mice with compromised DNA glycosylase activity [22,23], the overall features of prion disease were similar in *Neil2*$^{-/-}$ mice and wild-type mice. At the onset of disease, however, there was a tendency towards milder effects in *Neil2*$^{-/-}$ mice, with a lower disease score in the hypothalamus and lower levels of DNA damage, particularly in the spleen. Nevertheless, the *Neil2*$^{-/-}$ mice deteriorated very rapidly once clinical signs were evident and the synchronicity of these mice in reaching the clinical end-points suggested that they had reached a critical threshold, incompatible with neuronal survival. Interestingly, this occurred with such rapidity that the animals lost much less of their body mass than seen in the wild-type mice, in which the protracted clinical course included many days of anorexia.

Neil2 has been suggested to have a role in maintenance of the nuclear and mitochondrial genome [28]. In addition, mitochondrial dysfunction has been observed in brain of scrapie-infected mice [29,30]. Whereas mitochondrial functions, expressed as respiratory complex activity, remained unaffected in wild-type mice throughout the disease course, both in brain and spleen, the *Neil2*$^{-/-}$ mice appeared to mount a burst of mitochondrial activity in the spleen at end-stage. This was not evident in brain, in which activities were indistinguishable from wild-type mice. Recently, Neil2 was shown to protect the mitochondrial genome and prevent against mitochondrial-induced TP53 DNA damage response and intrinsic apoptosis during neural cell differentiation [31]. In contrast, we find that during prion infection loss of Neil2 prevents mitochondrial DNA damage and inhibits TP53 related pathways exclusively in spleen. This suggests that Neil2 may adopt organ-specific functions in a high oxidative stress environment. Spleen transcriptional responses also revealed a proliferative response in the *Neil2*$^{-/-}$ mice compared with the wild-type mice. Increased proliferation of cells could contribute to the observed increase in mitochondrial activity. The difference between the genotypes could in this regard, be influenced to some extent by the profound anorexia observed in the wild-type mice, which could initiate anorexia-mediated atrophy of the spleen. The proliferative response in the spleen could also contribute to potentially harmful pro-inflammatory signaling that could in turn, contribute to the rapid clinical deterioration of these animals.

Considering that the *Neil2*$^{-/-}$ mice have been shown to be in an induced state of innate immunity signaling and hyper-reactive towards inflammatory stimuli such as LPS and TNF-alpha [24] it is tempting to speculate that the loss of Neil2 accelerates toxic prion disease signaling and thereby leads to rapid death. However, the spleen morphology and follicular accumulation of PrP^{Sc} was quite similar between the genotype groups, with accumulations of what appeared to be amyloid masses in germinal centers. It has previously been reported that prion propagation (ME7 strain) in spleen can lead to disruption of the splenic follicular architecture [32], but this was not a prominent feature of our model, in which the general architecture of the spleen appeared intact even at end-stage prion disease.

We observed no difference in steady-state level of oxidative base lesions in brain and spleen of WT and *Neil2*$^{-/-}$ mice during prion progression. However, Neil2 is known to preferentially repair oxidized DNA bases from single-stranded DNA [33] and transcriptionally active genes [24]. Thus, we cannot exclude that gene-specific accumulation of DNA damage contributes to the observed phenotype. Notably, we found a diminished transcriptional response in *Neil2*$^{-/-}$ spleen during the course of disease suggesting that Neil2 is important for regulation of gene expression.

Interestingly, global levels of 5 mC changed significantly during

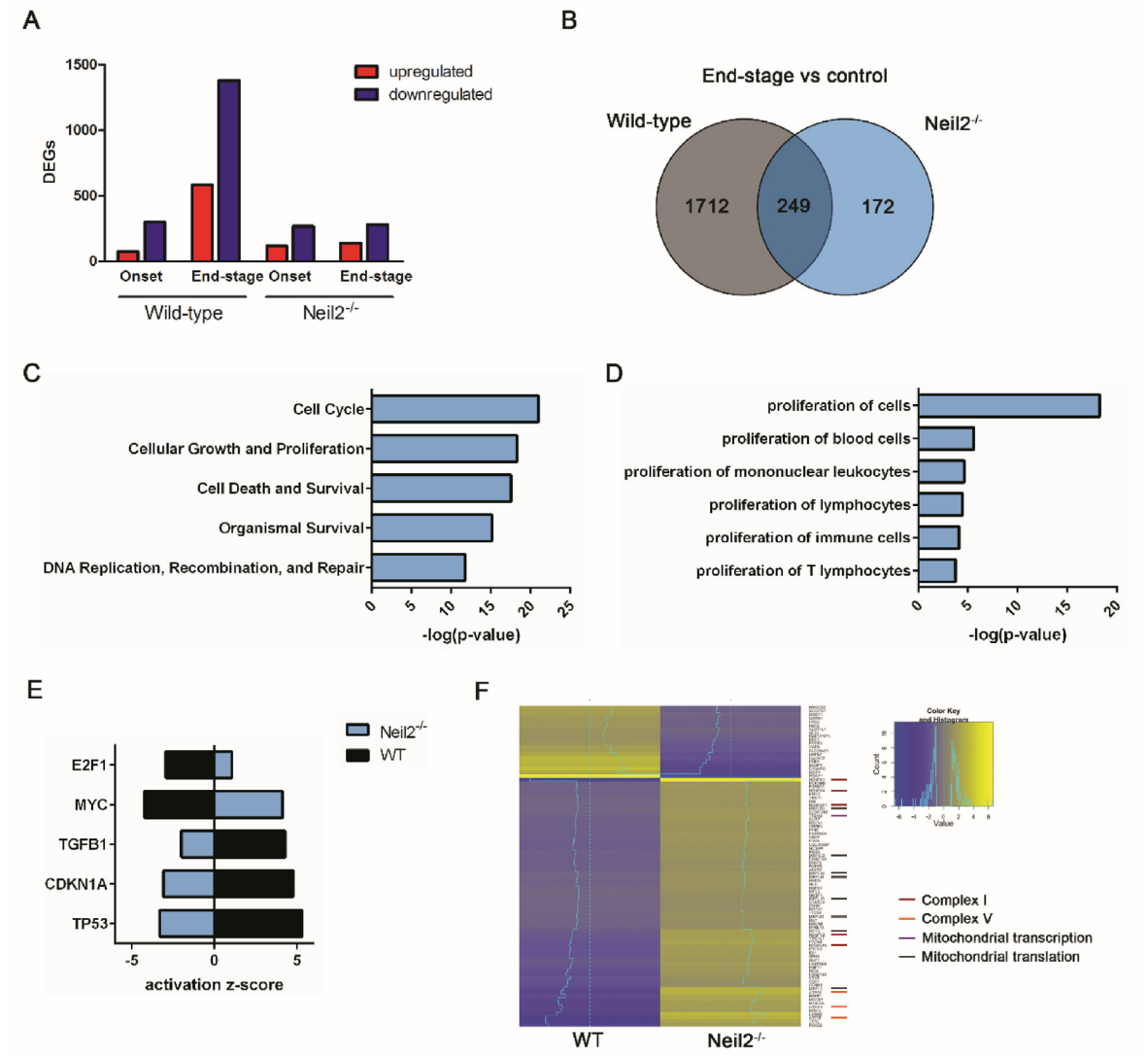

Fig. 4. RNA sequencing reveals enhanced proliferation of immune cells and increased expression of mitochondrial genes in spleen of *Neil2*$^{-/-}$ mice at end-stage of prion disease. A) Differentially expressed genes (DEGs) in wild-type (n = 4–6) and *Neil2*$^{-/-}$ (n = 4) spleen at onset and end-stage of prion disease, as compared with un-inoculated controls. B) Venn diagram showing overlap of DEGs at end-stage compared with controls from wild-type and *Neil2*$^{-/-}$ mice. Ingenuity pathway analysis showing C) Top five biological processes and D) biological processes involving proliferation enriched DEGs from *Neil2*$^{-/-}$ compared with wild-type mice at end-stage of prion disease. E) Activation score of top five upstream regulators enriched in DEGs from wild-type mice at end-stage compared with controls and DEGs from end-stage *Neil2*$^{-/-}$ mice compared with wild-type. F) Heatmap showing log2 fold change of DEGs involved in mitochondrial function from wild-type mice at end-stage compared to controls and end-stage *Neil2*$^{-/-}$ mice compared to wild-type.

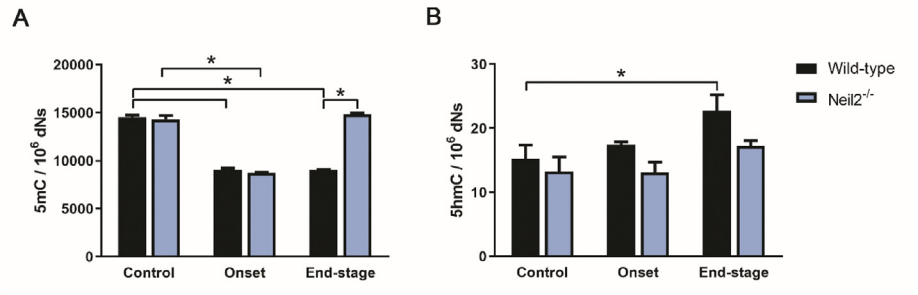

Fig. 5. *Neil2*$^{-/-}$ mice show increased DNA methylation levels in spleen at end-stage of prion disease. Mass spectrometry-based detection of genomic 5 mC and 5hmC in spleen of un-inoculated and RML-inoculated wild-type and *Neil2*$^{-/-}$ mice at onset and end-stage of disease. Data presented as means (n = 3–6 per group and time-point), +/− SEM. * (P < 0.05).

prion disease indicating an epigenetic mechanism as part of the pathogenesis. Besides its role in base lesion repair, Neil2 has been implicated in epigenetic gene regulation via active DNA demethylation [34,35]. Importantly, significant increased levels of 5 mC were found in *Neil2*$^{-/-}$ spleen at end-stage, supporting a potential role for Neil2 in epigenetic remodeling in the context of prion disease. However, delineating the mechanism requires deeper investigation in the future.

Taken together, our data suggest that distinct from detectable morphological alterations, and levels and distribution of PrP^{Sc} deposits, Neil2 activity counteracts toxic signaling in prion disease. This is in

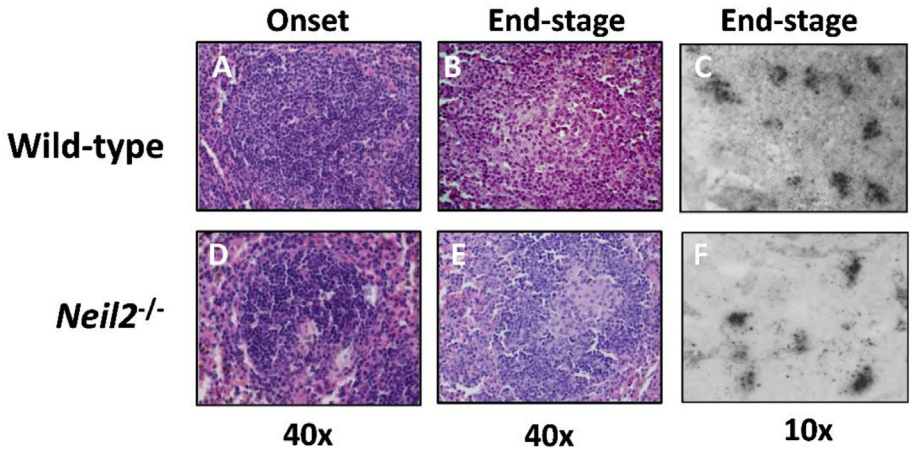

Fig. 6. Morphology of spleen lymphoid follicles and PrP^{Sc} accumulations at onset and end-stage prion disease. Haematoxylin eosin stained tissue sections of spleen lymphoid follicles from wild-type (panels A and B) and *Neil2*$^{-/-}$ (panels D and E) mice at onset and end-stage prion disease (magnification 40x). PrP^{Sc} follicular accumulation in spleen was visualized by paraffin-embedded tissue blots (Panels C and F), magnification 10x.

accordance with data demonstrating that Neil2, in contrast to OGG1, promotes anti-inflammatory signals.

Declaration of competing interest

The authors declare no competing financial interests.

Acknowledgments

We thank Dr. Andréoletti for the RML inoculum and the technical staff at the Norwegian Veterinary Institute for histopathological preparations. The authors greatly acknowledge Prof. Lucy Robertson for careful reading of the manuscript. This work was sponsored by the Research Council of Norway (FRIMEDBIO), the Central Norway Regional Health Authority and South-East Norway Regional Health Authority of Norway.

Appendix A. Supplementary data

Supplementary data to this article can be found online at https://doi.org/10.1016/j.freeradbiomed.2020.03.030.

Author contributions statement

KS, CMOJ, SLB, MB and MAT designed the study, performed experiments, analyzed data and wrote the manuscript. GG, TM and CE performed experiments and analyzed data. RS provided technical support, including mouse breeding and genetic analysis. All authors reviewed the manuscript.

References

[1] K.-M. Pan, et al., Conversion of alpha-helices into beta-sheets features in the formation of the scrapie prion proteins, Proc. Natl. Acad. Sci. Unit. States Am. 90 (23) (1993) 10962–10966.
[2] S.B. Prusiner, Molecular biology and pathogenesis of prion diseases, Trends Biochem. Sci. 21 (12) (1996) 482–487.
[3] W. Hadlow, R. Kennedy, R. Race, Natural infection of Suffolk sheep with scrapie virus, J. Infect. Dis. 146 (5) (1982) 657–664.
[4] C.I. Lasmézas, et al., Immune system-dependent and-independent replication of the scrapie agent, J. Virol. 70 (2) (1996) 1292–1295.
[5] K.L. Brown, et al., The effects of host age on follicular dendritic cell status dramatically impair scrapie agent neuroinvasion in aged mice, J. Immunol. 183 (8) (2009) 5199–5207.
[6] G. Millson, et al., Early distribution of radioactive liposomes and scrapie infectivity in mouse tissues following administration by different routes, Vet. Microbiol. 4 (2) (1979) 89–99.
[7] H. Fraser, A. Dickinson, Pathogenesis of scrapie in the mouse: the role of the spleen, Nature 226 (1970) 462–463.
[8] R.H. Kimberlin, C.A. Walker, Pathogenesis of experimental scrapie, Novel Infectious Agents and the Central Nervous System Ciba Foundation Symposium, 1988.
[9] R. Rubenstein, et al., Scrapie-infected spleens: analysis of infectivity, scrapie-associated fibrils, and protease-resistant proteins, JID (J. Infect. Dis.) 164 (1) (1991) 29–35.
[10] R. Race, et al., Diagnostic implications of detection of proteinase K-resistant protein in spleen, lymph nodes, and brain of sheep, Am. J. Vet. Res. 53 (6) (1992) 883–889.
[11] V. Béringue, et al., Facilitated cross-species transmission of prions in extraneural tissue, Science 335 (6067) (2012) 472–475.
[12] V. Béringue, et al., Prominent and persistent extraneural infection in human PrP transgenic mice infected with variant CJD, PloS One 3 (1) (2008) e1419.
[13] J. Chapuis, et al., Emergence of two prion subtypes in ovine PrP transgenic mice infected with human MM2-cortical Creutzfeldt-Jakob disease prions, Acta Neuropathol. Commun. 4 (1) (2016) 10.
[14] M. Jeffrey, et al., Sites of prion protein accumulation in scrapie-infected mouse spleen revealed by immuno-electron microscopy, J. Pathol. 191 (3) (2000) 323–332.
[15] L. McCulloch, et al., Follicular dendritic cell-specific prion protein (PrP C) expression alone is sufficient to sustain prion infection in the spleen, PLoS Pathog. 7 (12) (2011) e1002402.
[16] H. Krokan, R. Standal, G. Slupphaug, DNA glycosylases in the base excision repair of DNA, Biochem. J. 325 (1997) 1–16.
[17] H.E. Krokan, M. Bjørås, Base excision repair, Cold Spring Harb. Perspect. Biol. 5 (4) (2013) a012583.
[18] K. Scheffler, K.O. Bjoras, M. Bjoras, Diverse functions of DNA glycosylases processing oxidative base lesions in brain, DNA Repair 81 (2019) 102665.
[19] S. Xanthoudakis, et al., The redox/DNA repair protein, Ref-1, is essential for early embryonic development in mice, Proc. Natl. Acad. Sci. Unit. States Am. 93 (17) (1996) 8919–8923.
[20] E. Larsen, et al., Proliferation failure and gamma radiation sensitivity of Fen1 null mutant mice at the blastocyst stage, Mol. Cell Biol. 23 (15) (2003) 5346–5353.
[21] N. Puebla-Osorio, et al., Early embryonic lethality due to targeted inactivation of DNA ligase III, Mol. Cell Biol. 26 (10) (2006) 3935–3941.
[22] C.M.O. Jalland, et al., Accelerated clinical course of prion disease in mice compromised in repair of oxidative DNA damage, Free Radic. Biol. Med. 68 (2014) 1–7 0.
[23] C.M. Jalland, et al., Neil3 induced neurogenesis protects against prion disease during the clinical phase, Sci. Rep. 6 (2016).
[24] A. Chakraborty, et al., Neil2-null mice accumulate oxidized DNA bases in the transcriptionally active sequences of the genome and are susceptible to innate inflammation, J. Biol. Chem. 290 (41) (2015) 24636–24648.
[25] M. Bruce, A. Dickinson, Dementia and unconventional slow infections, Psychopharmacology of Old Age, 1982, pp. 15–23.
[26] R. Halsne, et al., Lack of the DNA glycosylases MYH and OGG1 in the cancer prone double mutant mouse does not increase mitochondrial DNA mutagenesis, DNA Repair 11 (3) (2012) 278–285.
[27] W. Wang, et al., Quantification of DNA damage by real-time qPCR, in: M. McKenzie (Ed.), Mitochondrial DNA: Methods and Protocols, Springer New York, New York, NY, 2016, pp. 27–32.
[28] S.M. Mandal, et al., Role of human DNA glycosylase Nei-like 2 (NEIL2) and single strand break repair protein polynucleotide kinase 3'-phosphatase in maintenance of mitochondrial genome, J. Biol. Chem. 287 (4) (2012) 2819–2829.
[29] H.-S. Choi, et al., Dysfunction of mitochondrial dynamics in the brains of scrapie-infected mice, Biochem. Biophys. Res. Commun. 448 (2) (2014) 157–162.
[30] J.H. Park, et al., Association of endothelial nitric oxide synthase and mitochondrial dysfunction in the hippocampus of scrapie-infected mice, Hippocampus 21 (3) (2011) 319–333.
[31] D. Han, et al., NEIL1 and NEIL2 DNA glycosylases protect neural crest development against mitochondrial oxidative stress, Elife 8 (2019).
[32] S. Kim, et al., Prion protein-deficient mice exhibit decreased CD4 T and LTi cell numbers and impaired spleen structure, Immunobiology 221 (1) (2016) 94–102.
[33] H. Dou, S. Mitra, T.K. Hazra, Repair of oxidized bases in DNA bubble structures by human DNA glycosylases NEIL1 and NEIL2, J. Biol. Chem. 278 (50) (2003) 49679–49684.
[34] L. Schomacher, et al., Neil DNA glycosylases promote substrate turnover by Tdg during DNA demethylation, Nat. Struct. Mol. Biol. 23 (2) (2016) 116–124.
[35] C.G. Spruijt, et al., Dynamic readers for 5-(hydroxy)methylcytosine and its oxidized derivatives, Cell 152 (5) (2013) 1146–1159.